Inorg. Chem. **2003**, *42*, 5274–5281

Magnetism of Cyano-Bridged Hetero-One-Dimensional Ln^{3+}–M^{3+} Complexes (Ln^{3+} = Sm, Gd, Yb; M^{3+} = Fe_{LS}, Co)

Albert Figuerola,[†] Carmen Diaz,*[,†] Joan Ribas,[†] Vassilis Tangoulis,[‡] Claudio Sangregorio,[§] Dante Gatteschi,[§] Miguel Maestro,[||] and José Mahía[||]

Departament de Química Inorgànica, Universitat de Barcelona, Martí i Franquès 1-11, 08028 Barcelona, Spain, Department of Materials Science, University of Patras, 26500 Patras, Greece, Department of Chemistry, University of Florence, UdR INSTM, Polo Scientifico Universitario, 50019 Sesto Fiorentino, Italy, and Servicios Xerais de Apoio a Investigación, Universidade da Coruña, Campus da Zapateira, s/n 15071, A Coruña, Spain

Received January 17, 2003

The reaction of $Ln(NO_3)_3$·aq with $K_3[Fe(CN)_6]$ or $K_3[Co(CN)_6]$ and 2,2′-bipyridine in water led to five one-dimensional complexes: *trans*-$[M(CN)_4(\mu\text{-}CN)_2Ln(H_2O)_4\ (bpy)]_n$·$XnH_2O$·1.5*n*bpy (M = Fe^{3+} or Co^{3+}; Ln = Sm^{3+}, Gd^{3+}, or Yb^{3+}; X = 4 or 5). The structures for [Fe^{3+}–Sm^{3+}] (**1**), [Fe^{3+}–Gd^{3+}] (**2**), [Fe^{3+}–Yb^{3+}] (**3**), [Co^{3+}–Gd^{3+}] (**4**), and [Co^{3+}–Yb^{3+}] (**5**) have been solved; they crystallize in the triclinic space $P\bar{1}$ and are isomorphous. The [Fe^{3+}–Sm^{3+}] complex is a ferrimagnet, its magnetic studies suggesting the onset of weak ferromagnetic 3-D ordering at 3.5 K. The [Fe^{3+}–Gd^{3+}] interaction is weakly antiferromagnetic. The isotropic nature of Gd^{3+} allowed us to evaluate the exchange interaction (J = 0.77 cm^{-1}).

Introduction

Paramagnetic lanthanide ions have attracted much interest in the field of molecule-based magnetic materials due to their large anisotropic magnetic moments.[1] Such magnetic anisotropy is required for magnetically ordered materials with large coercive fields. The origin of the magnetic anisotropy of lanthanides is the large unquenched orbital moment associated with the internal f magnetic orbitals. These contributions make the interpretation of the magnetic properties of these materials very difficult because the simple spin Hamiltonian schemes, which have been so successful for transition metal ions, break down. Associated with this is the fact that the magnetic interactions involving lanthanides are weak, and the crystal field effects on the magnetic susceptibility often mask them.

Therefore, no simple model is available for the interpretation of the magnetic properties of lanthanides analogous to those developed for transition metal ions (Goodenough–Kanamori rules,[2] Kahn–Briat[3] and Hay–Hoffmann[4] molecular orbital models, etc). Several attempts are currently underway to obtain compounds containing lanthanides coupled to transition metal ions[5−10] or organic radicals,[11−13] in the hope that this would increase the strength of the

* To whom correspondence should be addressed. E-mail: carme.diaz@qi.ub.es.
[†] Universitat de Barcelona.
[‡] University of Patras.
[§] University of Florence.
[||] Universidade da Coruña.

(1) (a) Benelli, C.; Gatteschi, D. *Chem. Rev.* **2002**, *102*, 2369. (b) de Sá, G. F.; Malta, O. P.; de Mello Donegá, C.; Simas, A. M.; Longo, R. L.; Santacruz, P. A.; da Silva, E. F., Jr. *Coord. Chem. Rev.* **2000**, *196*, 165 and references therein.
(2) Goodenough, J. B. *Magnetism and the Chemical Bond*; Interscience: New York, 1963.
(3) Kahn, O.; Briat, B. *J. Chem. Soc., Faraday Trans. 2* **1979**, *268*, 79.
(4) Hay, J. P.; Thibeault, J. C.; Hoffmann, R. *J. Am. Chem. Soc.* **1975**, *97*, 4884.
(5) (a) Costes, J. P.; Dahan, F.; Dupuis, A.; Laurent, J. P. *Inorg. Chem.* **2000**, *39*, 169. (b) Costes, J. P.; Dahan, F.; Dupuis, A.; Laurent, J. P. *Chem.—Eur. J.* **1998**, *9*, 1617.
(6) (a) Sanz, J. L.; Ruiz, L.; Gleizes, A.; Lloret, F.; Faus, J.; Julve, M.; Borras-Almenar, J. J.; Journaux, Y. *Inorg. Chem.* **1996**, *35*, 7384. (b) Deacon, G. B.; Forsyth, C. M.; Behrsing, T.; Konstas, K.; Forsyth, M. *Chem. Commun.* **2002**, 2820.
(7) (a) Bencini, A.; Benelli, C.; Canneschi, A.; Carlin, R. L.; Dei, A.; Gatteschi, D. *J. Am. Chem. Soc.* **1985**, *107*, 812. (b) Costes, J. P.; Clemente-Juan, J. M.; Dahan, F.; Dumestre, F.; Tuchagues, J. P. *Inorg. Chem.* **2002**, *41*, 2886.
(8) (a) Blake, A.; Milne, Winpenny, R. E. P. *Angew. Chem., Int. Ed. Engl.* **1991**, *30*, 1139. (b) Costes, J. P.; Dahan, F.; García-Tojal, J. *Chem.—Eur. J.* **2002**, *8*, 5430. (c) Chen, Q. Y.; Luo, Q. H.; Zheng, L. M.; Wanh, Z. L.; Chen, J. T. *Inorg. Chem.* **2002**, *41*, 605.
(9) (a) Liang, Y.; Cao, R.; Su, W.; Hong, M.; Zhang, W. *Angew. Chem., Int. Ed. Engl.* **2000**, *39*, 3304. (b) Gautier, R.; Andersen, O. K.; Gougeon, P.; Halet, J. F.; Canadell, E.; Martin, J. D. *Inorg. Chem.* **2002**, *41*, 4689.
(10) (a) Kahn, M. L.; Mathonière, C.; Kahn, O. *Inorg. Chem.* **1999**, *38*, 3692. (b) Kahn, M. L.; Lecante, P.; Verelst, M.; Mathoniere, C.; Kahn, O. *Chem. Mater.* **2000**, *12*,

10.1021/ic034051j CCC: $25.00
Published on Web 07/19/2003

magnetic interactions, on one hand, and halve the problem of orbital degeneracy, on the other. Hexacyanometalate complexes have been widely studied in the context of molecule-based magnets, in which the Prussian blue analogues show particularly fascinating magnetic properties, with high T_c values.[14] Research on cyano-bridged complexes has focused on transition metal ions.[15] With polycyanometalates and 4f ions several compounds with differing dimensionality have been reported.[16−30] With a focus on one-dimensional systems, some derivatives with polycyanometalates(II) (Ni, Pt)[20,21] or with polycyanometalates(III) (Fe, Co, Mn, Cr)[22−25] have been described.

We now report the synthesis, structures, and magnetic properties of compounds containing Gd^{3+}, for its orbital nondegeneracy, and Sm^{3+} and Yb^{3+}, as representatives of lanthanides with orbital moment, with the f configuration less and more than half-filled, respectively. Their formulas are the following (bpy = 2,2′-bipyridine): *trans*-$[Fe(CN)_4(\mu\text{-}CN)_2Sm(H_2O)_4(bpy)]_n\cdot 5nH_2O\cdot 1.5n$bpy (**1**); *trans*-$[Fe(CN)_4(\mu\text{-}CN)_2Gd(H_2O)_4(bpy)]_n\cdot 4nH_2O\cdot 1.5n$bpy (**2**); *trans*-$[Fe(CN)_4(\mu\text{-}CN)_2Yb(H_2O)_4(bpy)]_n\cdot 4nH_2O\cdot 1.5n$bpy (**3**); *trans*-$[Co(CN)_4(\mu\text{-}CN)_2Gd(H_2O)_4(bpy)]_n\cdot 4nH_2O\cdot 1.5n$bpy (**4**); *trans*-$[Co(CN)_4(\mu\text{-}CN)_2Yb(H_2O)_4(bpy)]_n\cdot 4nH_2O\cdot 1.5n$bpy (**5**). All these complexes are isomorphous, and they crystallize in the triclinic space $P\bar{1}$. The $[Fe^{3+}-Sm^{3+}]$ (**1**) complex is a ferrimagnet, magnetic studies suggesting the onset of weak ferromagnetic 3-D ordering at 3.5 K. In the $[Fe^{3+}-Gd^{3+}]$ (**2**) complex the interaction is weakly antiferromagnetic and the isotropic nature of Gd^{3+} allows the evaluation of the exchange interaction ($J = 0.77$ cm^{-1}). Together with the $[Fe^{3+}-Ln^{3+}]$ complexes, we attempted to synthesize and characterize the homologous $[Co^{3+}-Ln^{3+}]$ and $[Fe^{3+}-La^{3+}]$ complexes, to use the typical empirical approach developed by Costes et al.[5b] and previously used by the authors on the family of dinuclear $[Fe^{3+}-Ln^{3+}]$ complexes[17] to obtain insights into the nature of the $[Ln^{3+}-Fe^{3+}]$ coupling. The approach consists of comparing their magnetic susceptibility data with the corresponding isostructural $[Co^{3+}-Ln^{3+}]$ compounds, together with the magnetic properties of the $[Fe^{3+}-La^{3+}]$ complex, to take the anisotropy of the Fe^{3+} ion into account. The Co^{3+} and La^{3+} ions are obviously diamagnetic, and the deviation of the magnetic susceptibility of these compounds with respect to the Curie law is due entirely to the thermal population of the Ln^{3+} Stark components and the anisotropy of Fe^{3+}, respectively. It was impossible to apply this approach in all the complexes because when trying to synthesize the isostructural $[Co^{3+}-Sm^{3+}]$ and $[Fe^{3+}-La^{3+}]$ chains, new trinuclear complexes of formula $[Co(CN)_4(\mu\text{-}(CN)_2\{Sm(H_2O)_4(bpy)_2\}_2][Co(CN)_6]\cdot 8H_2O$ and $[Fe(CN)_4(\mu\text{-}(CN)_2\{La(H_2O)_4(bpy)_2\}_2][Fe(CN)_6]\cdot 8H_2O$ were obtained. The lack of isostructuralism prevented us from completing the mentioned approach.

Experimental Section

Materials. All starting materials were purchased from Aldrich and were used without further purification.

Synthesis of the New Complexes *trans*-$[Fe(CN)_4(\mu\text{-}CN)_2Sm(H_2O)_4(bpy)]_n\cdot 5nH_2O\cdot 1.5$nbpy (1), *trans*-$[Fe(CN)_4(\mu\text{-}CN)_2Gd(H_2O)_4(bpy)]_n\cdot 4nH_2O\cdot 1.5$nbpy (2), and *trans*-$[Fe(CN)_4(\mu\text{-}CN)_2Yb(H_2O)_4(bpy)]_n\cdot 4nH_2O\cdot 1.5$nbpy (3). The three $[Fe^{3+}-Ln^{3+}]$ complexes were obtained by adding a solution of $Ln(NO_3)_3\cdot nH_2O$ ($n = 5$, 6) (2.2 mmol) in water (15 mL) to an equimolar solution of $K_3[Fe(CN)_6]$ in water (50 mL). To this mixture an ethanolic solution (10 mL) of 2,2′-bipyridine (3.3 mmol) was added. The solutions were left undisturbed, and well-formed orange crystals were obtained, for all of them, after several days (yields ca. 70%). Anal. Calcd for **1**, $C_{31}H_{38}FeN_{11}O_9Sm$: C, 40.70; N, 16.84; H, 4.19. Found: C, 40.9; N, 17.0; H, 4.0. Calcd for **2**, $C_{31}H_{36}FeGdN_{11}O_8$: C, 41.20; N, 17.05; H, 4.01. Found: C, 41.1; N, 17.2; H, 3.9. Calcd for **3**, $C_{31}H_{36}FeN_{11}O_8Yb$: C, 40.49; N, 16.75; H, 3.95. Found: C, 40.6; N, 16.9; H, 3.9.

***trans*-$[Co(CN)_4(\mu\text{-}CN)_2Gd(H_2O)_4(bpy)]_n\cdot 4nH_2O\cdot 1.5$nbpy (4) and *trans*-$[Co(CN)_4(\mu\text{-}CN)_2Yb(H_2O)_4(bpy)]_n\cdot 4nH_2O\cdot 1.5$nbpy (5).** The two $[Co^{3+}-Ln^{3+}]$ complexes were obtained by the same procedure using $K_3[Co(CN)_6]$ instead of $K_3[Fe(CN)_6]$. Well-formed colorless crystals were obtained after several days (yields ca. 70%). Anal. Calcd for **4**, $C_{31}H_{36}CoGdN_{11}O_8$: C, 41.06; N, 16.99; H, 4.00. Found: C, 41.3; N, 17.1; H, 4.0. Calcd for **5**, $C_{31}H_{36}CoN_{11}O_8Yb$: C, 40.35; N, 16.70; H, 3.93. Found: C, 40.2; N, 16.8; H, 3.8.

Crystal Structure Determination. Crystal data and details on the data collection and refinement are summarized in Table 1. Suitable crystals of $[Fe^{3+}-Sm^{3+}]$ (**1**) (block, orange, dimensions $0.40 \times 0.35 \times 0.30$ mm^3), $[Fe^{3+}-Gd^{3+}]$ (**2**) (block, orange, dimensions $0.55 \times 0.50 \times 0.40$ mm^3), $[Fe^{3+}-Yb^{3+}]$ (**3**) (needle,

(11) (a) Sutter, J. P.; Kahn, M. L.; Golhen, S.; Ouahab, L.; Kahn, O. *Chem.—Eur. J.* **1998**, *4*, 571. (b) Lescop, C.; Belorizky, E.; Luneau, D.; Rey, P. *Inorg. Chem.* **2002**, *41*, 3375.
(12) (a) Canneschi, A.; Dei, A.; Gatteschi, D.; Sorace, L.; Vostrikova, K. *Angew. Chem., Int. Ed. Engl.* **2000**, *39*, 246 and references therein.
(13) (a) Kahn, M. L.; Sutter, J. P.; Golhen, S.; Guionneau, P.; Quahab, L.; Kahn, O.; Chasseau, D. *J. Am. Chem. Soc.* **2000**, *122*, 3413. (b) Lescop, C.; Luneau, D.; Rey, P.; Bussière, G.; Reber, C. *Inorg Chem.* **2002**, *41*, 5566.
(14) Verdaguer, M.; Bleuzen, A.; Train, C.; Garde, R.; Fabrizi De Biani, F.; Desplanches, C. *Philos. Trans. R. Soc. London, Ser. A* **1999**, *357* (1762), 2959.
(15) (a) Ohba, M.; Okawa, H. *Coord. Chem. Rev.* **2000**, *198*, 313. (b) Cernák, J.; Orendác, M.; Potocnák, I.; Chomic, J.; Orendacová, A.; Skorsepa, J.; Feher, A. *Coord. Chem. Rev.* **2002**, *224*, 51.
(16) (a) Huliger, F.; Landolt, M.; Vetsch, H. *J. Solid State Chem.* **1976**, *18*, 307. (b) Huliger, F.; Landolt, M.; Vetsch, H. *J. Solid State Chem.* **1976**, *18*, 283.
(17) Figuerola, A.; Diaz, C.; Ribas, J.; Tangoulis, V.; Granell, J.; Lloret, F.; Mahía, J.; Maestro, M. *Inorg. Chem.* **2002**, *42*, 641.
(18) Kou, H. Z.; Gao, S.; Jin, X. *Inorg. Chem.* **2001**, *40*, 6295.
(19) Ma, B. Q.; Gao, S.; Su, G.; Xu, G. X. *Angew. Chem., Int. Ed.* **2001**, *40*, 434.
(20) Knoeppel, D. W.; Liu, J.; Meyers, E. A.; Shore, S. G. *Inorg. Chem.* **1998**, *37*, 4828.
(21) Du, B.; Ding, E.; Meyers, E. A.; Shore, S. G. *Inorg.Chem.* **2001**, *40*, 3637.
(22) Yan, B.; Wang, H. D.; Chen, Z. D. *Polyhedron* **2001**, *20*, 591.
(23) Yan, B.; Chen, Z.; Wang, S.; Gao, S. *Chem. Lett.* **2001**, 350.
(24) (a) Tanase, S.; Andruh, M.; Müller, A.; Schmidtmann, M.; Mathonière, C.; Rombaut, G. *Chem. Commun.* **2001**, 1084. (b) Gao, S.; Su, G.; Yi, T.; Ma, B. Q. *Phys. Rev. B* **2001**, *63*, 054431.
(25) (a) Figuerola, A.; Diaz, C.; Ribas, J.; El. Falah, M. S.; Maestro, M.; Mahía, J. *Chem. Commun.* **2001**, 1204. (b) Kou, H. Z.; Gao, S.; Li, C. H.; Liao, D. Z.; Zhou, B. C.; Wang, R. J.; Li, Y. *Inorg. Chem.* **2002**, *41*, 4756.
(26) (a) Yan, B.; Chen, Z. *Helv. Chim. Acta* **2001**, 817. (b) Yan, B.; Chen, Z. *Transition Met. Chem.* **2001**, *26*, 287.
(27) Liu, S.; Meyers, E. A.; Shore, S. G. *Angw. Chem., Int. Ed.* **2002**, *41*, 3609.
(28) Kautz, J. A.; Mullica, D. F.; Cunningham, B. P.; Combs, R. A.; Farmer, J. M. *J. Mol. Struct.* **2000**, *523*, 175.
(29) Kou, H. Z.; Yang, G. M.; Liao, D. Z.; Cheng, P.; Jiang, Z. H.; Yan, S. P.; Huang, X. Y.; Wang, G. L. *J. Chem. Crystallogr.* **1998**, *28*, 303.
(30) Mullica, D. F.; Farmer, J. M.; Cunningham, B. P.; Kautz, J. A. *J. Coord. Chem.* **2000**, *49*, 239.

Table 1. Crystal Parameters for **1**−**5**

	[Fe^{3+}−Sm^{3+}] (**1**)	[Fe^{3+}−Gd^{3+}] (**2**)	[Fe^{3+}−Yb^{3+}] (**3**)	[Co^{3+}−Gd^{3+}] (**4**)	[Co^{3+}−Yb^{3+}] (**5**)
empirical formula	$C_{31}H_{38}FeN_{11}O_9Sm$	$C_{31}H_{36}FeGdN_{11}O_8$	$C_{31}H_{36}FeN_{11}O_8Yb$	$C_{31}H_{36}CoGdN_{11}O_8$	$C_{31}H_{36}CoN_{11}O_8Yb$
formula mass	914.92	903.81	919.60	906.89	922.68
space group	$P\bar{1}$	$P\bar{1}$	$P\bar{1}$	$P\bar{1}$	$P\bar{1}$
cryst system	triclinic	triclinic	triclinic	triclinic	triclinic
Z	2	2	2	2	2
a, Å	9.744(1)	9.708(1)	9.715(1)	9.706(1)	9.664(2)
b, Å	10.672(1)	10.604(1)	10.584(1)	10.601(1)	10.584(3)
c, Å	19.750(3)	19.690(1)	19.756(1)	19.752(1)	19.798(3)
α, deg	82.932(2)	82.821(1)	83.313(1)	82.980(1)	83.45(1)
β, deg	83.524(2)	83.657(1)	84.391(1)	83.784(1)	84.37(1)
γ, deg	64.624(2)	64.372(1)	63.894(1)	64.272(1)	63.88(1)
V, Å^3	1837.4(4)	1809.5(1)	1809.1(1)	1813.8(1)	1803.8(7)
ρ(calc), g/cm^3	1.654	1.659	1.688	1.661	1.699
μ_{calc}, mm^{-1}	2.044	2.282	3.034	2.334	3.101
radiation (Mo Kα), Å	0.710 73	0.710 73	0.710 73	0.710 73	0.710 73
T, K	173(2)	173(2)	173(2)	173(2)	173(2)
final R indices[a]	R1 = 0.0291	R1 = 0.0300	R1 = 0.0281	R1 = 0.0297	R1 = 0.0357
[$I > 2\sigma(I)$]	wR2 = 0.0776	wR2 = 0.0755	wR2 = 0.0661	wR2 = 0.0751	wR2 = 0.0828
final R indices	R1 = 0.0320	R1 = 0.0326	R1 = 0.0337	R1 = 0.0321	R1 = 0.0395
(for all data)	wR2 = 0.0791	wR2 = 0.0768	wR2 = 0.0687	wR2 =0.0764	wR2 = 0.0842

[a] $R1 = \sum||F_o| - |F_c||/\sum|F_o|$ and $wR2 = \{\sum[w(F_o^2 - F_c^2)^2]/\sum[w(F_o^2)^2]\}^{1/2}$.

orange, dimensions 0.55 × 0.10 × 0.10 mm^3), [Co^{3+}−Gd^{3+}] (**4**) (block, colorless, dimensions 0.55 × 0.50 × 0.30 mm^3), and [Co^{3+}−Yb^{3+}] (**5**) (block, colorless, dimensions 0.55 × 0.50 × 0.30 mm^3) were used for the structure determination. X-ray data were collected using a Bruker SMART CCD area detector single-crystal diffractometer with graphite-monochromatized Mo Kα radiation (λ = 0.710 73 Å) by the $\phi-\omega$ scan method at 173(2) K. A total of 1271 frames of intensity data were collected for each compound. The first 50 frames were collected at the end of data collection to monitor for decay. In each case, the crystals used for the diffraction studies showed no decomposition during data collection. The integration process yields a total of 12 961 reflections for **1**, 12 470 for **2**, 12 440 for **3**, 12 499 for **4**, and 12 126 for **5** of which 8862 [R(int) = 0.0236], 8555[R(int) = 0.0199], 8591[R(int) = 0.0222], 8596 [R(int) = 0.0190], and 8665 [R(int) = 0.0397], respectively, were independent. Absorption corrections were applied using SADABS[31] program (maximum and minimum transmission coefficients: 0.5348 and 0.4598 for **1**; 0.462 and 0.367 for **2**; 0.751 and 0.286 for **3**; 0.541 and 0.360 for **4**; 0.456 and 0.280 for **5**). The structures were solved using the Bruker SHELXTL-PC[32] software by direct methods and refined by full-matrix least-squares methods on F^2. Hydrogen atoms were included in calculated positions and refined in the riding mode, less those of water molecules that were located on residual density maps, but their positions were then fixed and they were refined in the riding mode. For **1** convergence was reached at a final R1 = 0.0291 [for $I > 2\sigma(I)$], wR2 = 0.0791 (for all data), 607 parameters, with allowance for the thermal anisotropy for all non-hydrogen atoms. The weighting scheme employed was $w = [\sigma^2(F_o^2 + (0.0514P)^2 + 2.4048P]$ and $P = (|F_o|^2 + 2|F_c|^2)/3$, and the goodness of fit on F^2 was 0.953 for all observed reflections. For **2** convergence was reached at a final R1 = 0.0300 [for $I > 2\sigma(I)$], wR2 = 0.0768 (for all data), 488 parameters, with allowance for the thermal anisotropy for all non-hydrogen atoms. The weighting scheme employed was $w = [\sigma^2(F_o^2 + (0.0528P)^2]$ and $P = (|F_o|^2 + 2|F_c|^2)/3$, and the goodness of fit on F^2 was 1.018 for all observed reflections. For **3** convergence was reached at a final R1 = 0.0281 [for $I > 2\sigma(I)$], wR2 = 0.0687 [for all data], 488 parameters, with allowance for the thermal anisotropy for all non-hydrogen atoms. The weighting scheme employed was $w = [\sigma^2(F_o^2 + (0.0355P)^2]$ and $P = (|F_o|^2 + 2|F_c|^2)/3$, and the goodness of fit on F^2 was 1.005 for all observed reflections. For **4** convergence was reached at a final R1 = 0.0297 [for $I > 2\sigma(I)$], wR2 = 0.0764 (for all data), 488 parameters, with allowance for the thermal anisotropy for all non-hydrogen atoms. The weighting scheme employed was $w = [\sigma^2(F_o^2 + (0.0531P)^2]$ and $P = (|F_o|^2 + 2|F_c|^2)/3$, and the goodness of fit on F^2 was 1.033 for all observed reflections. For **5** convergence was reached at a final R1 = 0.0357 [for $I > 2\sigma(I)$], wR2 = 0.0842 (for all data), 488 parameters, with allowance for the thermal anisotropy for all non-hydrogen atoms. The weighting scheme employed was $w = [\sigma^2(F_o^2 + (0.0106P)^2]$ and $P = (|F_o|^2 + 2|F_c|^2)/3$, and the goodness of fit on F^2 was 1.016 for all observed reflections.

Physical Measurements. Magnetic susceptibilities were measured on polycrystalline powders with a Cryogenic S600 SQUID magnetometer. Powders were pressed in a pellet to prevent preferential crystallite orientation with the magnetic field. HF-EPR spectra were recorded on a laboratory made spectrometer using as radiation source a Gunn diode operating at 95 GHz equipped with a second harmonic generator.

Results and Discussion

Description of the Structures of *trans*-[$Fe(CN)_4$-(μ-$CN)_2Sm(H_2O)_4$(bpy)]$_n$·5nH_2O·1.5nbpy (1), *trans*-[$Fe(CN)_4$(μ-$CN)_2Gd(H_2O)_4$(bpy)]$_n$·4nH_2O·1.5nbpy (2), *trans*-[$Fe(CN)_4$(μ-$CN)_2Yb(H_2O)_4$(bpy)]$_n$·4nH_2O·1.5nbpy (3), *trans*-[$Co(CN)_4$(μ-$CN)_2Gd(H_2O)_4$(bpy)]$_n$·4nH_2O·1.5nbpy (4), and *trans*-[$Co(CN)_4$(μ-$CN)_2Yb(H_2O)_4$(bpy)]$_n$·4nH_2O·1.5nbpy (5). The structure of these complexes was determined by X-ray crystallography. In all five cases, the crystal system is triclinic with space group $P\bar{1}$. Their crystallographic analysis revealed that they all confine isomorphous one-dimensional (1-D) chain polymers. An ORTEP view of [Fe^{3+}−Yb^{3+}] (**3**) complex with the atom-labeling scheme is given in Figure 1. Selected bond lengths and angles for **1**−**5** are listed in Table 2. As an example a projection of the chains for [Fe^{3+}−Gd^{3+}] (**2**) complex in the *xy* plane is shown in Figure 2. The chains show an alternation of Ln^{3+} ion and

(31) Sheldrick, G. M. *SADABS*; University of Göttingen: Göttingen, Germany, 1996. This is a program for absorption corrections using Bruker CCD data.
(32) Sheldrick, G. M. *Bruker SHELXTL-PC*; University of Göttingen: Göttingen, Germany, 1997.

Table 2. Selected Bond Lengths (Å) and Angles (deg) for **1**−**5**

	$[Fe^{3+}-Sm^{3+}]$ (**1**)	$[Fe^{3+}-Gd^{3+}]$ (**2**)	$[Fe^{3+}-Yb^{3+}]$ (**3**)	$[Co^{3+}-Gd^{3+}]$ (**4**)	$[Co^{3+}-Yb^{3+}]$ (**5**)
Ln(1)−O(1)	2.434(2)	2.404(2)	2.356(2)	2.417(2)	2.365(3)
Ln(1)−O(2)	2.382(2)	2.343(2)	2.276(2)	2.352(2)	2.283(2)
Ln(1)−O(3)	2.444(2)	2.411(2)	2.344(2)	2.413(2)	2.340(2)
Ln(1)−O(4)	2.406(2)	2.378(2)	2.323(2)	2.380(2)	2.318(3)
Ln(1)−N(1)	2.529(2)	2.488(2)	2.426(3)	2.508(2)	2.449(3)
Ln(1)−N(4)	2.511(2)	2.466(2)	2.405(3)	2.490(2)	2.418(3)
Ln(1)−N(7)	2.561(2)	2.533(2)	2.475(3)	2.536(2)	2.473(3)
Ln(1)−N(8)	2.595(2)	2.571(2)	2.508(2)	2.571(2)	2.510(3)
M(1)−C(1)	1.939(3)	1.936(3)	1.948(3)	1.905(2)	1.918(4)
M(1)−C(2)	1.949(3)	1.941(3)	1.951(3)	1.903(3)	1.908(4)
M(1)−C(3)	1.941(3)	1.934(3)	1.939(3)	1.899(3)	1.900(4)
M(1)−C(4)	1.932(3)	1.927(3)	1.937(3)	1.898(2)	1.906(4)
M(1)−C(5)	1.940(3)	1.942(3)	1.955(3)	1.901(3)	1.905(4)
M(1)−C(6)	1.954(3)	1.952(3)	1.957(3)	1.912(2)	1.914(4)
C(1)−N(1)	1.154(3)	1.151(3)	1.163(4)	1.153(3)	1.159(5)
Ln(1)−N(1)−C(1)	175.5(2)	175.4(2)	175.9(2)	175.3(2)	175.5(3)
M(1)−C(1)−N(1)	176.2(2)	175.8(2)	175.5(3)	175.8(2)	175.6(3)

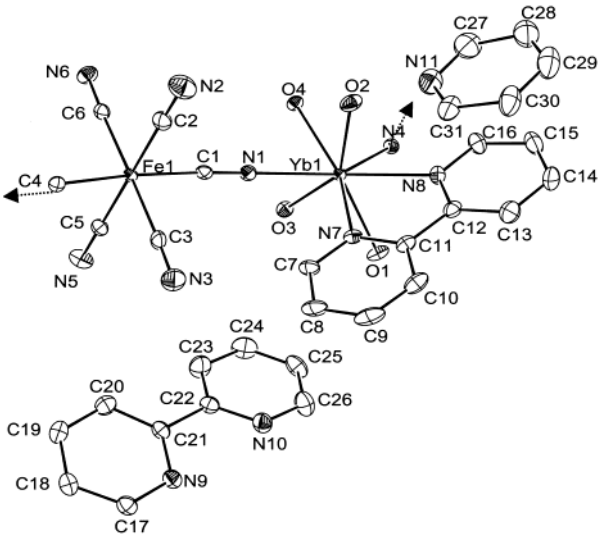

Figure 1. ORTEP view of complex *trans*-$[Fe(CN)_4(\mu\text{-}CN)_2Yb(H_2O)_4(bpy)]_n \cdot 4nH_2O \cdot 1.5n$bpy (**3**) with atom labeling scheme. Complexes **1**, **2**, **4**, and **5** show a similar structure (they are isostructural).

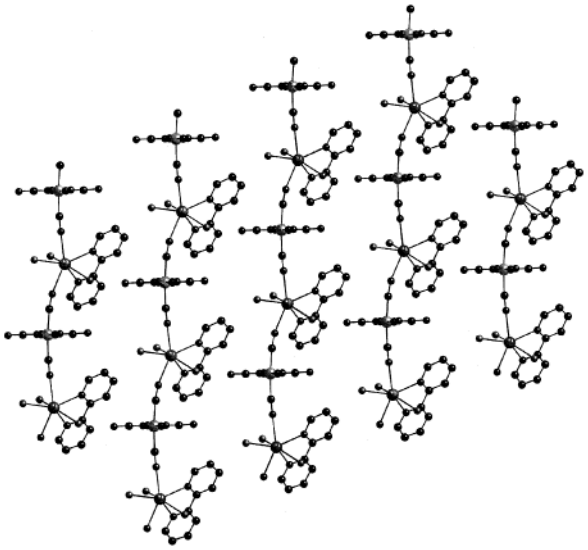

Figure 2. Schematic representation of the packing of the chains of *trans*-$[Fe(CN)_4(\mu\text{-}CN)_2Gd(H_2O)_4(bpy)]_n \cdot 4nH_2O \cdot 1.5n$bpy (**2**) in the *xy* plane. Complexes **1**, **3**, **4**, and **5** show similar packing.

$[M(CN)_6]^{3-}$ (M = Fe, Co) units linked by cyanide bridges in the trans geometry. The coordination sphere around the Ln^{3+} ion comprises two nitrogen atoms of 2,2′-bipyridine ligand, four oxygen atoms of four water molecules, and two nitrogen atoms of the cyanide bridges. The eight-coordinated Ln^{3+} ion lies in a distorted dodecahedral environment. The distances Ln−O range from 2.45 to 2.27 Å. The lowest values are observed for Yb^{3+} in accordance with the variation of the radius of the lanthanide ions. Six cyanide ligands surround the M^{3+} (Co, Fe) ion in a distorted octahedral environment. The M−C distances range from 1.88 to 1.96 Å, and the lowest correspond to the $[Co(CN)_6]^{3-}$. The Ln−M (M = Fe, Co) intramolecular distances are: 5.612 Å for **1**, 5.564 Å for **2**, 5.421 Å for **3**, 5.555 Å for **4**, and 5.515 Å for **5**. The Ln−M−Ln angle are 159.55° for **1**, 159.40° for **2**, 159.17° for **3**, 159.40° for **4,** and 159.27° for **5**, indicating the trans geometry. A projection of the $[Fe^{3+}-Gd^{3+}]$ complex (**2**) in the *yz* plane is shown in Figure 3; between the chains there are water molecules and bipyridine crystallization molecules. It is interesting to note that the bpy of crystallization adopts two different stereo configurations. One of

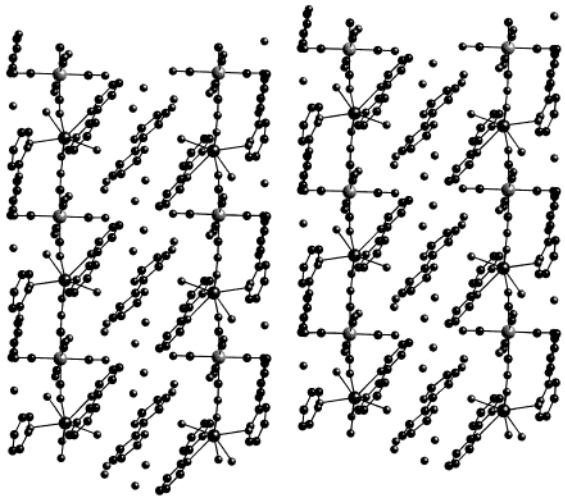

Figure 3. View of the packing of *trans*-$[Fe(CN)_4(\mu\text{-}CN)_2Gd(H_2O)_4(bpy)]_n \cdot 4nH_2O \cdot 1.5n$bpy (**2**) in the *yz* plane. Complexes **1**, **3**, **4**, and **5** show similar packing.

them is not planar, showing a dihedral angle (N−C−C−N) of 18° for **1**, 17.5° for **2**, 16.6° for **3**, 17.4° for **4**, and 16.6°

Table 3. Distances between bpy Rings Centroids (Å)[a]

	$[Fe^{3+}-Sm^{3+}]$ (**1**)	$[Fe^{3+}-Gd^{3+}]$ (**2**)	$[Fe^{3+}-Yb^{3+}]$ (**3**)	$[Co^{3+}-Gd^{3+}]$ (**4**)	$[Co^{3+}-Yb^{3+}]$ (**5**)
Cg(1)−Cg(5)	3.564	3.560	3.612	3.580	3.631
Cg(2)−Cg(5)	3.620	3.595	3.609	3.596	3.612
Cg(3)−Cg(4)	3.869	3.837	3.826	3.836	3.830

[a] Cg(1) ring of N(7); Cg(2) ring of N(8); Cg(3) ring of N(9); Cg(4) ring of N(10); Cg(5) ring of N(11).

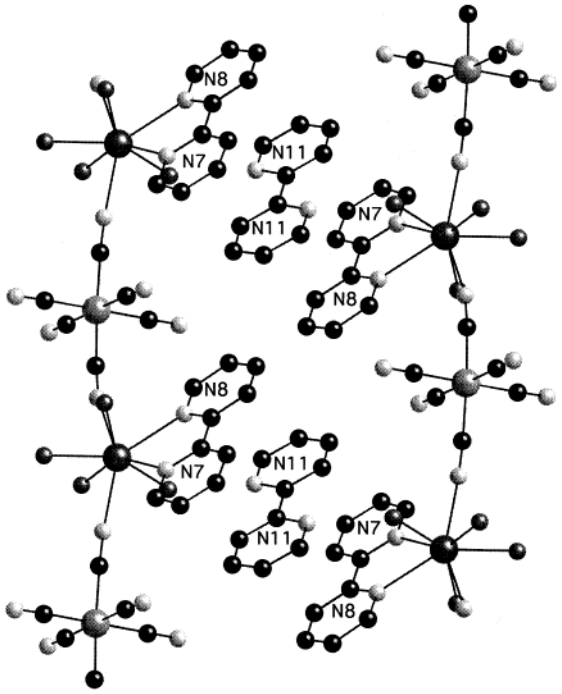

Figure 4. Schematic representation of the $\pi-\pi$ interactions of *trans*-$[Fe(CN)_4(\mu\text{-}CN)_2Gd(H_2O)_4(bpy)]_n\cdot 4nH_2O\cdot 1.5n$bpy (**2**) in the *yz* plane. Complexes **1**, **3**, **4**, and **5** show similar $\pi-\pi$ interactions.

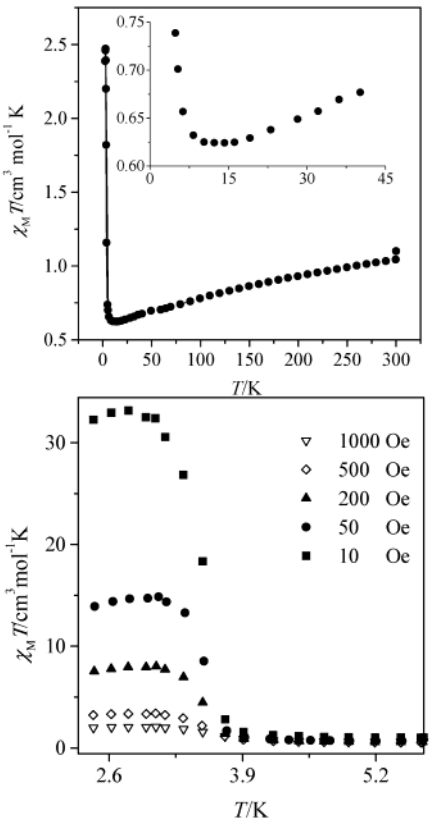

Figure 5. Top: Thermal dependence at 0.1 T of $\chi_M T$ for $[Fe^{3+}-Sm^{3+}]$ (**1**). Bottom: Thermal dependence at different low fields (from 1000 to 10 Oe) of $\chi_M T$ for $[Fe^{3+}-Sm^{3+}]$ (**1**).

for **5**; the other configuration is planar but the same dihedral angle is 180°. Bond lengths and angles of the bpy ligand are similar to those observed in the free bpy molecules, taking into account the abnormal *trans* configuration. Hydrogen bonds involving the nitrogen atoms of the bpy of crystallization, the four oxygen atoms of the H_2O ligands of the $Ln(H_2O)_4(bpy)$ entity, the nitrogen atoms of the terminal CN^- ligands of the $M(CN)_6$ entity, and the water molecules of crystallization provide additional stabilization of the crystal structure, giving an extensive 3-D network. The *trans*-bpy of crystallization and the bpy ligands of two neighboring chains exhibit a weak $\pi-\pi$ interaction (Figure 4). A $\pi-\pi$ interaction between each of two neighboring nonplanar bpy of crystallization is also present in the crystal. Intermolecular stacking distances between centroids of the bpy rings are shown for all complexes in Table 3.

Magnetic Studies. Magnetic measurements were performed for the five $[Fe^{3+}-Ln^{3+}]$ and $[Co^{3+}-Ln^{3+}]$ complexes. The lanthanide (with the exception of Gd^{3+}) and Fe^{3+} ions possess a first-order angular momentum, which prevents the use of a spin-only Hamiltonian for isotropic exchange.

$[Fe(CN)_4(\mu\text{-}CN)_2Sm(H_2O)_4(bpy)]_n\cdot 5nH_2O\cdot 1.5n$bpy (1). The temperature dependence of $\chi_M T$ of the $[Fe^{3+}-Sm^{3+}]$ compound is shown at the top of Figure 5. The $\chi_M T$ value is about 1.10 cm^3 mol^{-1} K at 300 K; it reaches a minimum of 0.62 cm^3 mol^{-1} K at approximately 15 K (inset of Figure 5, top) and then increases drastically to 2.5 cm^3 mol^{-1} K at 2 K. The behavior of the system is analogous to that observed in ferrimagnets. Low-temperature magnetic measurements were carried out to understand this behavior. Susceptibility measurements were carried out at a range of low magnetic fields (Figure 5, bottom). When the magnetic field decreased from 1000 to 10 Oe, the maximum susceptibility increased from 2.5 to 33 cm^3 mol^{-1} K. ZFC-FC measurements at 50 Oe indicate the onset of weak ferromagnetic 3-D ordering at 3.5 K possibly due to interchain interactions mediated by hydrogen bonds and/or $\pi-\pi$ stacking (Figure 6, top). To confirm the onset of the ordering, hysteresis was measured at 2 K. The region from −0.15 to +0.15 T for 2 and 2.5 K is shown for clarity (Figure 6, bottom). The coercivity at 2 K is ca. 137 Oe, and the remnant magnetization is $M_R = 0.08\ N\mu_B$ while, at 2.5 K, the values are 60 Oe and 0.06 $N\mu_B$.

To confirm that the long-range ordering reported in complex **1** is not due to impurity trace of the 3-D compound $Sm[Fe(CN)_6]\cdot 4H_2O$ published by Hulliguer et al.,[16b] a comparison of X-ray diffraction patterns was made. In Figures S1 and S2 (Supporting Information), the powder

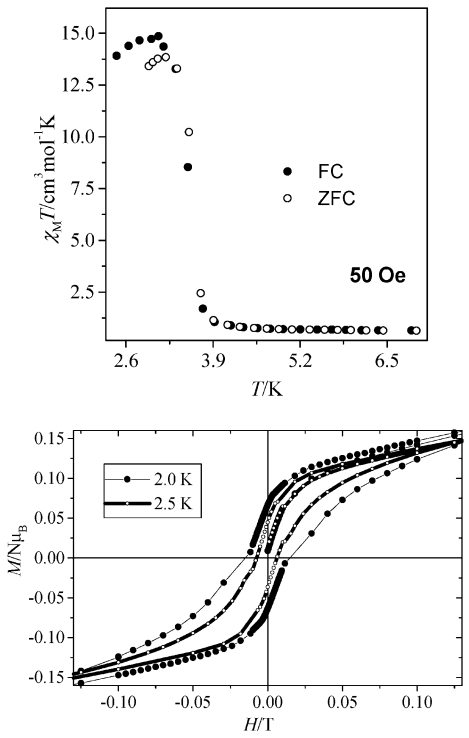

Figure 6. Top: Temperature dependence of $\chi_M T$ for [$Fe^{3+}-Sm^{3+}$] (**1**) cooled in zero-field (ZFC) and in a field of 50 Oe (FC). Bottom: Hysteresis cycle at 2.0 and 2.5 K for [$Fe^{3+}-Sm^{3+}$] (**1**).

X-ray diffraction patterns of **1** and $Sm[Fe(CN)_6]\cdot 4H_2O$ complexes, in the range $2\theta = 12-55°$ at room temperature, are shown. The calculated X-ray patterns from the CIF files for both complexes (Figure S3 and S4) are according with the experimental ones. The superposition of the experimental X-ray diffraction patterns, in all the 2θ range and in the $2\theta = 12-25$ range where the $Sm[Fe(CN)_6]\cdot 4H_2O$ complex presents the most intense peaks (Figures S5 and S6, Supporting Information), indicates that no significant impurity trace of compound $Sm[Fe(CN)_6]\cdot 4H_2O$ was found. These results are in good agreement with those of the elemental analysis.

$[Fe(CN)_4(\mu\text{-}CN)_2Gd(H_2O)_4(bpy)]_n\cdot 4nH_2O\cdot 1.5nbpy$ (2) and $[Co(CN)_4(\mu\text{-}CN)_2Gd(H_2O)_4(bpy)]_n\cdot 4nH_2O\cdot 1.5nbpy$ (4). The magnetic behavior of the [$Co^{3+}-Gd^{3+}$] compound follows the Curie law with $\chi_M T$ value equal to 7.77 cm^3 mol^{-1} K, which corresponds to an isolated Gd^{3+} ion. The temperature dependence of the $\chi_M T$ of the [$Fe^{3+}-Gd^{3+}$] compound at 0.1 and 1 T is shown at the top of Figure 7. At 300 K, $\chi_M T$ is approximately equal to 8.4 cm^3 mol^{-1} K while it differs for the two fields at lower temperature. At 0.1 T it reaches a minimum of 7.5 cm^3 mol^{-1} K at 3.5 K and then increases to 8.0 cm^3 mol^{-1} K at 2 K. The same figure shows that no minimum is observed for the susceptibility data at 1 T. The behavior of the system is ferrimagnetic while at high fields (1 T) there is no minimum in the susceptibility data (inset of Figure 7) but a continuous decrease due to field saturation and/or zero field splitting. To investigate the magnitude of the magnetic interactions in the [$Gd^{3+}-Fe^{3+}$] a fit of the data at 0.1 T was made using a model for a chain of alternating classic (7/2) and quantum (1/2) spins. The

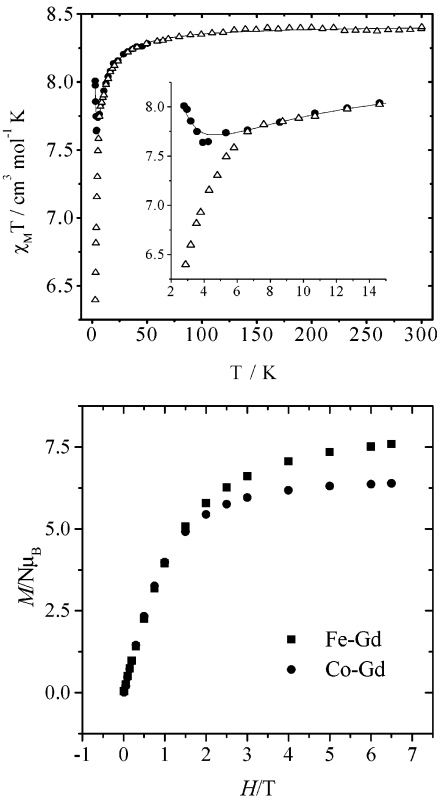

Figure 7. Top: Thermal dependence at 0.1 T (●) and 1 T (△) of $\chi_M T$ for [$Fe^{3+}-Gd^{3+}$] (**2**). Bottom: Magnetization vs H for [$Fe^{3+}-Gd^{3+}$] (**2**) and for [$Co^{3+}-Gd^{3+}$] (**4**) at 2 K.

Hamiltonian employed was[33]

$$H = J\sum_{i=1}^{N-1}[S_{(i)} + S_{(i+1)}]s_{(i)} \quad S_{(i)} = 7/2,\ s_{(i)} = 1/2$$

A satisfactory fit was obtained with $J = 0.77$ cm^{-1} and $g = 2.0$. The anisotropy of the $Fe^{3+}{}_{LS}$ was not taken into consideration and so the above model is an approximation, but it nevertheless reflects the weak ferrimagnetic behavior of the system.[33] The field dependence of the magnetization of compounds [$Gd^{3+}-Fe^{3+}$] and [$Gd^{3+}-Co^{3+}$] is shown at the bottom of Figure 7.

$[Fe(CN)_4(\mu\text{-}CN)_2Yb(H_2O)_4(bpy)]_n\cdot 4nH_2O\cdot 1.5nbpy$ (3) and $[Co(CN)_4(\mu\text{-}CN)_2Yb(H_2O)_4(bpy)]_n\cdot 4nH_2O\cdot 1.5nbpy$ (5). The temperature dependence of $\chi_M T$ for complex [$Fe^{3+}-Yb^{3+}$] is shown at the top of Figure 8. At 300 K, the $\chi_M T$ value is approximately equal to 3.2 cm^3 mol^{-1} K while it decreases with temperature to 2.1 cm^3 mol^{-1} K at 2 K. The temperature dependence of $\chi_M T$ for the [$Co^{3+}-Yb^{3+}$] compound is also shown at the top of Figure 8. At 300 K, the $\chi_M T$ value is approximately equal to 2.5 cm^3 mol^{-1} K, close to the expected value for one isolated Yb^{3+} ion (2.57 cm^3 mol^{-1} K), and decreases smoothly with temperature to 1.6 cm^3 mol^{-1} K at 2 K. The lack of the characterization of the isostructural [$Fe^{3+}-La^{3+}$] prevents the approach indicated above to deduce the sign of the magnetic coupling between

(33) Press, W. H.; Flannery, B. P.; Teukolsky, S. A.; Vetterling, W. T. *Numerical Recipes: The Art of Scientific Computing*; Cambridge University Press: Cambridge, U.K., 1986; Chapter 14.4.

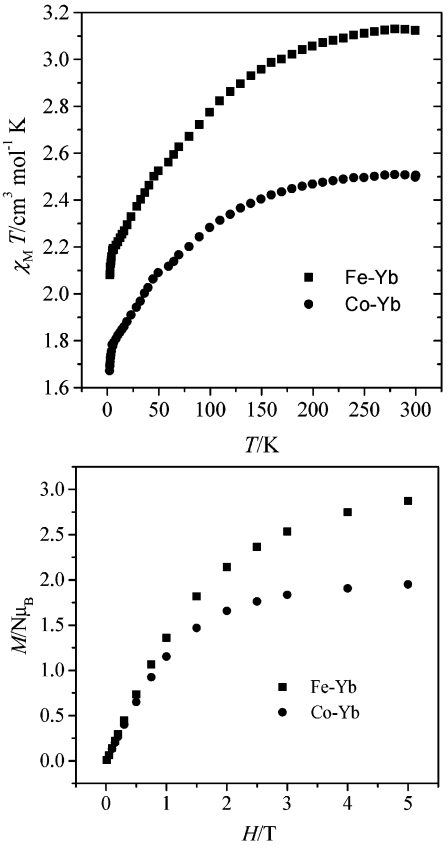

Figure 8. Top: Thermal dependence at 0.1 T of $\chi_M T$ for (**3**) and $\chi_M T$ for [$Co^{3+}-Yb^{3+}$] (**5**). Bottom: Magnetization vs H for [$Fe^{3+}-Yb^{3+}$] (**3**) and [$Co^{3+}-Yb^{3+}$] (**5**) at 2 K.

Fe^{3+} and Yb^{3+} (if any). When we attempted the synthesis of this isostructural one-dimensional complex, a new completely different trinuclear [$La^{3+}-Fe^{3+}-La^{3+}$] complex was obtained (see Introduction). The field dependence of the magnetization of compounds [$Fe^{3+}-Yb^{3+}$] and [$Co^{3+}-Yb^{3+}$] at 2 K is shown at the bottom of Figure 8.

HF-EPR Studies. [$Fe(CN)_4(\mu\text{-}CN)_2Gd(H_2O)_4(bpy)]_n \cdot 4nH_2O \cdot 1.5nbpy$ (2) and [$Co(CN)_4(\mu\text{-}CN)_2Gd(H_2O)_4(bpy)]_n \cdot 4nH_2O \cdot 1.5nbpy$ (4). The temperature dependence of the spectrum of [$Gd^{3+}-Co^{3+}$] at 95 GHz is shown at the top of Figure 9. The spectrum is typical of an $S = 7/2$ spin system with a small zero-field-splitting parameter. A simulation of the spectrum[34] at 10 K was carried out according to the Hamiltonian formalism

$$H = \mathrm{SDS} + \mu_\beta H g_i S_i$$

and the following parameters were obtained: $D = 0.093$ cm^{-1}; $E = 0.030$ cm^{-1}; $g = 1.99$. The simulation is shown in Figure 10, where a rhombic signal with small zero-field parameter can be observed. The temperature dependence of [$Fe^{3+}-Gd^{3+}$] system at 190 GHz is shown at the bottom of Figure 9. Many features appear around the central derivative at ca. 7 T, while an interesting g-shift occurs, expanding the satellites at both lower and higher magnetic fields. This is

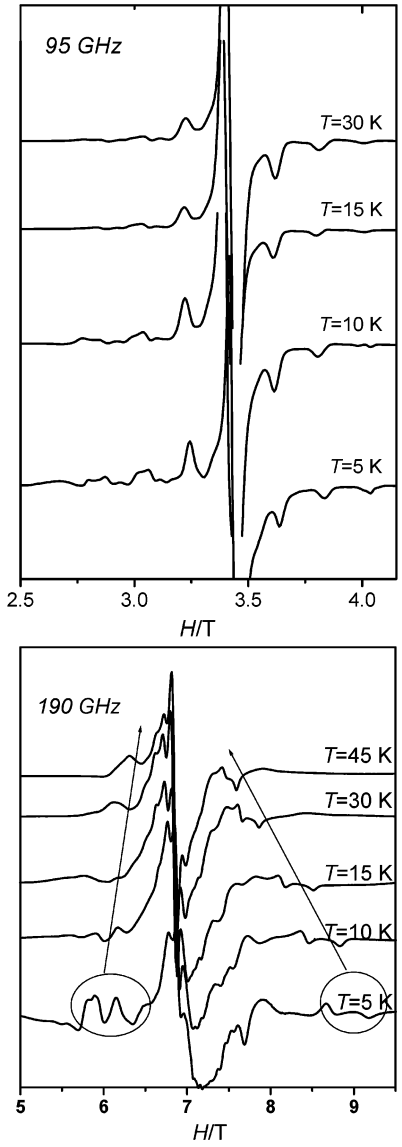

Figure 9. Top: EPR spectra at 95 GHz and a range of temperatures for [$Co^{3+}-Gd^{3+}$] (**4**). Bottom: EPR spectra at 190 GHz and a range of temperatures for [$Fe^{3+}-Gd^{3+}$] (**2**).

expected for 1-D systems, where short-range effects occur due to dipolar interchain interactions.[35] Further single-crystal anisotropic magnetic and EPR measurements are underway to explore the anisotropic magnetic interactions in these systems.

Conclusions

Five one-dimensional [$Fe^{3+}(Co^{3+})-Ln^{3+}$] complexes have been structurally characterized and magnetically studied (Ln^{3+} = Sm^{3+}, Gd^{3+}, Yb^{3+}). All five are isostructural, the nature of the metal ion being the only change introduced. Long-range magnetic ordering was observed for the [$Fe^{3+}-Sm^{3+}$] compound with a T_c equal to 3.5 K and a coercive field of 137 Oe at 2 K. Most of the 3d−4f complexes reported in the literature that show long-range magnetic ordering involve the Sm^{3+} ion. Indeed, Hulliguer et al. pub-

(34) The program to simulate the EPR spectra has been kindly provided by H. Weihe, Institute of Chemistry, Odense Universitet, Odense M, Denmark.

(35) Gatteschi, D.; Bencini, A. *EPR of Exchange Coupled Systems*, Springer-Verlag: Berlin, Heidelberg, 1990.

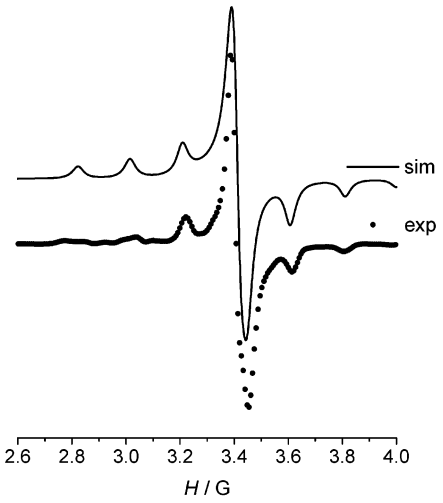

Figure 10. Simulation of the EPR at 10 K for $[Co^{3+}-Gd^{3+}]$ (**4**).

lished a tridimensional compound of formula $Sm[Fe(CN)_6]\cdot 4H_2O$ with T_c equal to 3.5 K and a coercitive field of 5 KOe at 1.3 K;[16b] Gao et al. published a bidimensional structure of formula $[Sm(DMF)_2(H_2O)_3Cr(CN)_6]\cdot H_2O$ with T_c equal to 4.2 K and a coercive field of 100 Oe at 1.85 K[18] and a one-dimensional one of formula $[Sm(DMF)_4(H_2O)_2Mn(CN)_6]_n\cdot nH_2O$ which showed a $T_c = 18$ K and a $H_c = 600$ Oe at 5.7 K;[23] Chen et al. published a new one-dimensional compound with formula $\{[Sm(DMA)_2(H_2O)_4Fe(CN)_6]\cdot 5H_2O\}_n$ (DMA = *N*,*N*′-dimethylacetamide) with $T_c = 3.5$ K and $H_c = 1400$ Oe at 1.8K.[26a] The replacement of the Sm^{3+} ion by another lanthanide ion usually gives rise to isostructural compounds that lose all three-dimensional magnetic properties, when the dimensionality is low. The long-range magnetic ordering observed in the $[Fe^{3+}-Sm^{3+}]$ chain presented in this article could be due to the hydrogen bonding and/or the presence of $\pi-\pi$ interactions between the chains. The T_c for **1** and $Sm[Fe(CN)_6]\cdot 4H_2O$ is approximately the same. In principle the T_c for interacting 1-D compounds should be less than that in the 3-D compounds. The results of the comparative study of the X-ray diffraction patterns allow us to confirm the long-range order in complex **1**. The explanation of this similar T_c is not easy, but we should take into account that in the 3-D system the magnetic interaction through the CN^- bridged ligands are quite small and hydrogen bonds are also present. The synthesis of new Sm^{3+} complexes is necessary to check this tendency to give long-range magnetic ordering. Finally, a low antiferromagnetic interaction was observed for the $[Fe^{3+}-Gd^{3+}]$ complex ($J = 0.77$ cm^{-1}) and it was impossible to determine the sign of the magnetic coupling for the $[Fe^{3+}-Yb^{3+}]$ complex.

Acknowledgment. Grant BQU2000/0791 supported this study from the Dirección General de Investigación Científica y Técnica (Spanish Government). We also thank Nicola Lima, Dipartimento di Chimica, Università degli Studi di Firenze, for providing us the program based on ref 33 to fit the $[Fe^{3+}-Gd^{3+}]$ complex and Lorenzo Sorace, CNRS-LCMI 25, Grenoble, France, for the measurements of the HF-EPR spectra.

Supporting Information Available: Five X-ray crystallographic files in CIF format and X-ray diffraction patterns (Figures S1−S6). This material is available free of charge via Internet at http//pubs.acs.org.

IC034051J